

MHD theory of the solar tachocline with meridional flow

A. Sule, G. Rüdiger, and R. Arlt

Astrophysikalisches Institut Potsdam, An der Sternwarte 16, D-14482, Potsdam, Germany

Received date / Accepted date

Abstract. It has been shown that the best explanation for the formation of the tachocline is that of magnetic nature. We present here the first simulations of the solar tachocline, which self-consistently include the meridional circulation. We show that the meridional circulations significantly change the shape and the characteristics of the tachocline. We find that after the inclusion of the meridional circulations, a tachocline can be formed even when the poloidal field lines are crossing the boundary between the radiative zone and the convection zone. We also discuss the effects of the magnetic Prandtl number as well as of the magnetic Reynolds number on the properties of the tachocline. The tachocline is much thinner for the higher magnetic Reynolds numbers and/or lower magnetic Prandtl numbers. We expect a poloidal magnetic seed field of around 0.1 G will be sufficient to produce a tachocline in the Sun. The simulations including the temperature gradient produce shallower as well as slower meridional circulations than the ones without it, as desired from Lithium abundance in the solar convection zone.

Key words. MHD – Sun:interior – Sun: magnetic fields – Sun: rotation

1. Introduction

The term tachocline refers to a very thin layer at the base of the convection zone, which separates the latitudinal differential rotation inside the convection zone from the uniformly rotating radiative zone. Latest observational estimates put the position of its center around $0.69R_{\odot}$ and estimate its thickness to be slightly less than $0.05R_{\odot}$. There is also general belief that the tachocline is prolate and is also thicker near the pole. However, the observations for higher latitudes have large error bars, and hence the evidence for the latitudinal dependence of the tachocline is no way conclusive (Schou et al. 1998, Antia et al. 1998, Charbonneau et al. 1999, Basu & Antia 2001). The same can be qualitatively verified in frequency-versus-radius plots presented in recent works (Eff-Darwich et al. 2002, Howe 2003).

There have been many attempts to explain the formation of such a thin shear layer inside the Sun. Spiegel & Zahn (1992) were the first to give a purely hydrodynamic model for the tachocline. But it was realized that in a hydrodynamic case, turbulent stresses will make the tachocline thicker over time, and finally the entire Sun will start rotating differentially. Even the later works as that of Miesch (2003) confirm that a purely hydrodynamic model is insufficient to explain the tachocline.

Rüdiger & Kitchatinov (1997) studied the tachocline under the influence of a magnetic field. They believed that

the existence of a weak seed field ($\sim 1\text{--}100\ \mu\text{G}$) in the solar core is highly likely. And this weak internal magnetic field will be mainly responsible for the formation of the tachocline. Many others like Gough & McIntyre (1998), MacGregor & Charbonneau (1999) and Garaud (2002) have used this idea of a weak poloidal seed field forming the tachocline.

Here we present a magnetohydrodynamic model, which self-consistently calculates the meridional flow. In this work, we show how the inclusion of the meridional circulations changes the shape of the tachocline and discuss the effect of varying magnetic Prandtl number and magnetic Reynolds number on the structure and the properties of the tachocline. Finally, we discuss the effect of the temperature gradient on the structure of the meridional flow.

For a very simple magnetic shear flow model the relation

$$\frac{\delta R}{R} \propto \text{Ha}^{-1/2} \quad (1)$$

has been derived by Rüdiger & Kitchatinov (1997) for the fractional thickness of any magnetic-induced tachocline layer with the Hartmann number

$$\text{Ha} = \frac{B_0 R}{\sqrt{\mu_0 \rho \nu \eta}}, \quad (2)$$

so that rather thin transitions of (say) 0.03 always require $\text{Ha} \simeq 10^3$. The Hartmann number also appears in the

relation between the induced toroidal magnetic field B_ϕ and the given poloidal field amplitude B_0 , i.e.

$$\frac{B_\phi}{B_0} \simeq \frac{\Omega(\delta R)^2}{\eta} \simeq \frac{\text{Rm}}{\text{Ha}} \quad (3)$$

(the amplification factor) with the global magnetic Reynolds number $\text{Rm} = \Omega R^2/\eta$.

With $\eta \simeq 10^3 \text{ cm}^2/\text{s}$ one finds $\text{Rm} \simeq 10^{12}$ for the solar transition region between the convection zone and the radiative interior so that the very strong amplification of nine (!) orders of amplitudes should occur. The code used below only reaches Rm -values of order 10^5 so that only small amplifications can be reached.

Forgács-Dajka & Petrovay (2002) and Petrovay (2003) suggest that the tachocline, being just below the base of the convection zone, is more likely to be turbulent and hence the values of the diffusivities in this region are more likely to be as high as those in the convection zone. Some previous works concentrate on the stability of the tachocline being subject to the latitudinal shear (Watson 1981, Gilman & Fox 1997, Garaud 2001, Cally 2003, Dikpati et al. 2003). These ideas, however, are beyond the scope of present discussion.

2. The model

The principle aim of this work will be to reproduce the observed rotation profile in the tachocline region, along with the rotation profile in the solar radiative zone below.

To remain consistent with the observations, we require that (i) the thickness of the tachocline should be less than $0.05R_\odot$, (ii) the core should achieve near uniform rotation, (iii) the meridional circulations should be slow and/or should not be penetrating deep in the radiative zone, and (iv) the internal seed field should be weak.

We assume that the tachocline lies completely inside the radiative zone. The equations take the simple, axisymmetric, incompressible, Boussinesq form. We take the outer radius of the computational domain as $R_{\text{out}} = 0.75R_\odot$ and the inner radius as $R_{\text{in}} = 0.1R_\odot$. We also assume that the rotation profile in the convection zone is independent of the dynamics in the radiative zone and can be prescribed as a boundary condition. We further assume that any physical phenomenon occurring in the convection zone, including the dynamos, do not bear effect on the dynamics within the radiative zone and the tachocline. For the first set of simulations, the effect of the temperature gradient and hence buoyancy force on the fluid is also neglected. We will present the equations involving the temperature in the subsequent discussion.

The magnetohydrodynamic equations are

$$\frac{\partial \mathbf{u}}{\partial t} = -(\mathbf{u} \cdot \nabla)\mathbf{u} - \nabla P + \nu \nabla^2 \mathbf{u} + \frac{1}{\mu_0 \rho} (\nabla \times \mathbf{B}) \times \mathbf{B}, \quad (4)$$

$$\frac{\partial B_\phi}{\partial t} = [\nabla \times (\mathbf{u} \times \mathbf{B})]_\phi - \eta [\nabla \times (\nabla \times \mathbf{B})]_\phi \quad (5)$$

with $\nabla \cdot \mathbf{u} = 0$ and $\nabla \cdot \mathbf{B} = 0$ where ν and η are the viscosity (here constant) and the magnetic diffusivity (here

constant), respectively. Other symbols have their usual meaning. The poloidal magnetic field is maintained time-invariant. This approximation is valid as in the Sun, due to extremely small η , the magnetic diffusion time is about a order higher than the present solar age, whereas, the stable tachocline solution is reached in our simulations in far shorter times.

The equations are to be solved in a spherical shell geometry using the spectral code developed by Hollerbach (1994) and Hollerbach (2000). For convenience the equations are scaled in time by the magnetic diffusion time, $\tau_{\text{diff}} = R_{\text{out}}^2/\eta$, in velocity by η/R_{out} , and the magnetic field in the form of a Lundquist number, i.e.

$$S_0 = \frac{B_0 R_{\text{out}}}{\sqrt{\mu_0 \rho} \eta}. \quad (6)$$

This reduces the equations to very few free parameters, namely $r_{\text{out}} = R_{\text{out}}/R_\odot$, $r_{\text{in}} = R_{\text{in}}/R_\odot$, Rm , $\text{Pm} = \nu/\eta$ and S_0 .

The rotation profile of the angular velocity at the outer boundary is chosen to match the observed rotation profile in the bulk of the convection zone, which is also used by MacGregor & Charbonneau (1999) and is maintained as a rigid boundary condition. It is given by

$$\Omega_{\text{out}} = \Omega_0 (1 - 0.1264 \cos^2 \theta - 0.1591 \cos^4 \theta), \quad (7)$$

where θ is the co-latitude. The remaining boundary conditions on the velocity are maintained stress-free. For the magnetic field, we assume vacuum boundary conditions at the inner as well as the outer boundary.

Due to the computational limitations, we will use more moderate values of Rm not exceeding 10^5 . We believe that the magnetic diffusivity (η) and the viscosity (ν) take their molecular values in the tachocline region but our choice of Rm , due to the numerical constraints, means in our computations we have used very high values of η and ν .

The computations using the 2D spectral code are done with typically 60 Chebyshev (k) modes and 60 Legendre (l) modes. It has been verified by additional computations that in the simple cases presented here, the results are independent of the resolution chosen.

The magnetic field structure used for the internal seed field is dipolar with no initial toroidal field. i.e.

$$\mathbf{B} = \left(\frac{1}{r^2 \sin \theta} \frac{\partial A}{\partial \theta}, -\frac{1}{r \sin \theta} \frac{\partial A}{\partial r}, 0 \right) \quad (8)$$

with

$$A = S_0 r^2 \left(1 - \frac{r}{r_{\text{out}}} \right) \left(1 - \frac{r_{\text{in}}}{r} \right) \sin^2 \theta \quad (9)$$

where A is the magnetic vector potential. Different authors have previously used different vector potentials for the simulations. We will use the expressions of A as given in Charbonneau & MacGregor (1993) and used by MacGregor & Charbonneau (1999)¹.

¹ The Charbonneau & MacGregor (1993) model was for a complete sphere whereas our simulations deal with spherical

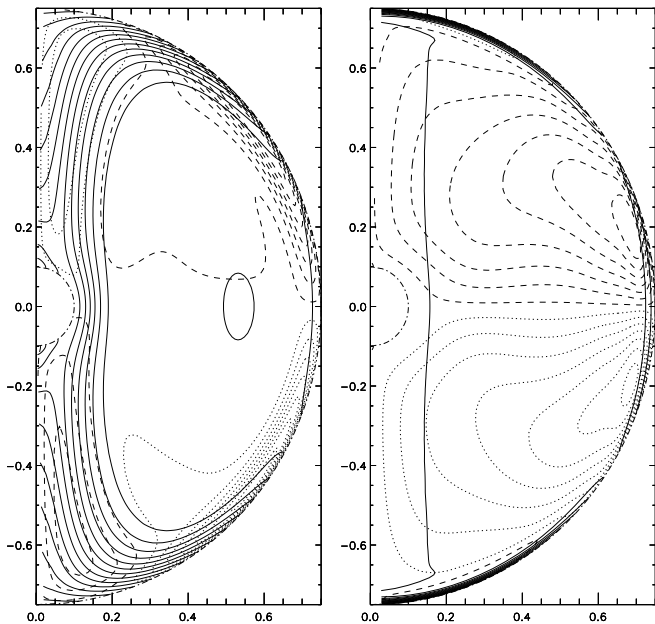


Fig. 1. Results for the simulations excluding (left) and including (right) meridional circulations, when the magnetic field is confined to the core. The solid lines are the iso-rotation curves, whereas the dashed and the dotted lines represent the contours of the positive and the negative toroidal field strength respectively. The dot-dashed lines indicate the boundaries of the simulation domain. The time-invariant poloidal magnetic field is not shown. $S_0 = 1100$, $Pm = 1$ and $Rm = 10^4$.

3. The effect of the meridional flow

The earlier works have shown that even a weak seed poloidal field is able to produce a solar-like tachocline. It was found that the region near the rotation axis (i.e. poles) is least affected and the tachocline is thickest in that part. Further, when the poloidal field amplitude is very small, the magnetic field is unable to affect the rotation profile and the resulting rotation profile looks very similar to the non-magnetic case. Also, when the magnetic field strength is very high, the contour lines of constant Ω follow the poloidal magnetic field lines throughout the interior, in accordance with Ferraro's (1937) theorem. Hence a solar-like tachocline, in either case, is impossible (Garaud 2002). Our simulations in absence of the meridional flow concur with the most of these key results.

In the simulations in this section, we use $Rm = 10^4$ and $Pm = 1$. The results are best represented by the comparison of the following two figures. While the left panel of Fig. 1 is just a reproduction of the earlier MacGregor & Charbonneau (1999) result, where the magnetic fields

shells. Hence an extra term is incorporated in the vector potential to avoid the magnetic fields crossing the inner boundary. This will mean that the poloidal magnetic field is no more curl-free. We eliminate the curl of the poloidal magnetic field, which is dominant only at the inner boundary, by equating it to zero at every time step.

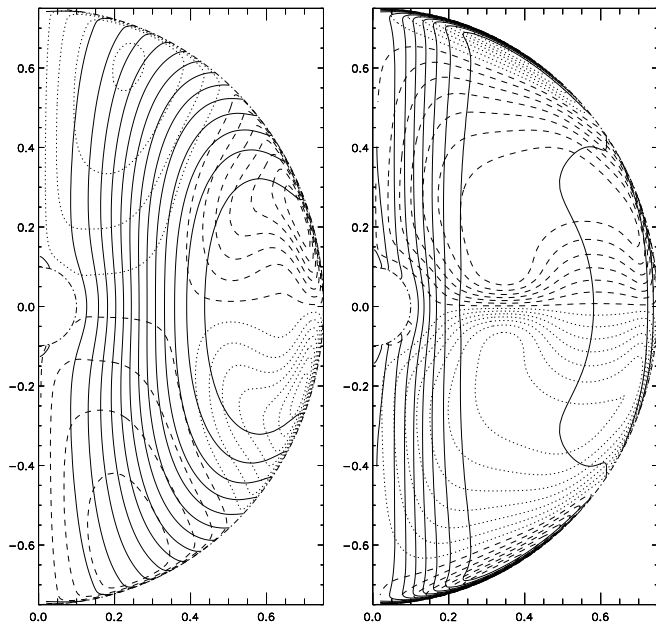


Fig. 2. Results for the simulations excluding (left) and including (right) the meridional circulations when the magnetic field lines are crossing the outer boundary.

are confined to the simulation domain, the right panel of Fig. 1 shows the same model with the inclusion of the meridional circulations. The solid lines are the iso-rotation curves whereas the dashed and the dotted lines represent the contours of the positive and the negative toroidal field strength respectively. We see that while in the figure on the left, the region along the rotation axis is not affected at all, the inclusion of the meridional circulation changes the picture completely.

We observe that the entire core, including the region near the rotation axis, has achieved near uniform rotation. The tachocline is formed near the outer boundary. Contrary to the results without meridional flow, the tachocline is thinnest near the pole. In the region near the equator, where the magnetic field is not influencing much, we see that the iso-rotation curves tend to be similar to the characteristic Taylor-Proudman flow. We further observed that the toroidal magnetic field strength is only 30% of the poloidal magnetic field strength.

Similar to MacGregor & Charbonneau (1999), we also studied the second case, where the poloidal magnetic field is no more confined to the computational domain and the magnetic field lines are crossing the outer boundary of the simulation domain. While this case produced no real tachocline for the MacGregor & Charbonneau (1999) model, after inclusion of the meridional flows, this is no longer a problem (see Fig. 2).

We performed some test simulations with a decaying poloidal magnetic field. During these simulations, we observed that initially the magnetic field forms a tachocline but as the magnetic field decays gradually due to the high value of η assumed in the simulations, the flows readjust themselves, and the resulting pattern will be the same as

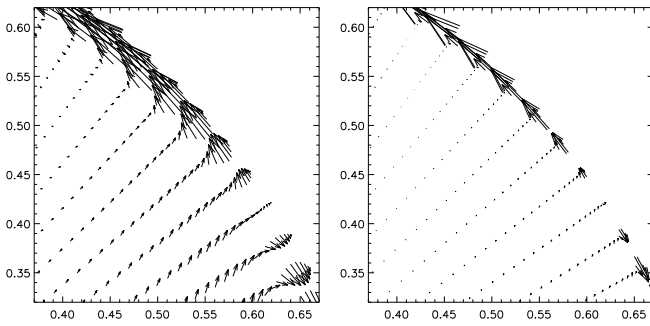


Fig. 3. Results for the simulations with $Pm = 1$ (left) and 0.05 (right) showing a small section of the simulation domain with the components of the meridional circulation plotted. Lengths of the arrows are proportional to the amplitude of the flow. Only alternate points in the radial direction are plotted to avoid congestion.

the purely hydrodynamic case, i.e. it will approach the Taylor-Proudman flow.

We conclude here that the magnetic field is not only important for the formation of the tachocline but is also important for maintaining it, at least in case of the high magnetic diffusivity used in these simulations.

4. Effect of varying magnetic Prandtl number and magnetic Reynolds number

4.1. Varying the magnetic Prandtl number

Following Kippenhahn & Weigert (1994) and Stix & Skaley (1990), the solar value for the magnetic Prandtl number is of the order of 10^{-3} . Though achieving this value was not possible, simulations were performed for various values of Pm in the range of $1-0.05$ whereas $Rm = 10^4$ in all the cases.

In these simulations, we observed that the horizontal component of the meridional flow (u_θ) generated is about 2% of u_ϕ at higher latitudes and is about 1% for lower latitudes. Similarly, the vertical component of the meridional flow (u_r) is about 0.5% (see Fig. 4 left). These ratios are nearly independent of the value of the Pm . The radial component of the velocity remains much smaller than the latitudinal component especially at lower values of Pm , as seen in Fig. 3. Also as seen in Fig. 3, strong latitudinal flows are expelled closer to the outer boundary at lower values of Pm . The tachocline, thus formed, is thinner² at the pole than at the equator. The thickness of the tachocline at the equator reduces marginally from $0.030R_\odot$ to $0.026R_\odot$ when Pm is changed from 1 to 0.05, whereas the thickness of the tachocline at the pole decreases considerably. We also observe that the amplitude of the toroidal magnetic field remains smaller than that of

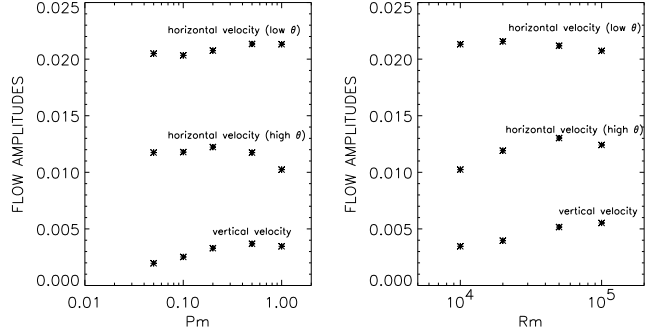


Fig. 4. The amplitudes of the components of the meridional flow at different co-latitudes (θ), normalized to the rotational velocity at the equator, with varying Pm (left) and Rm (right).

the poloidal field and is almost independent of the choice of Pm .

4.2. Varying the magnetic Reynolds number

Now we will use the constant $Pm = 1$ and vary Rm . As we know that the solar value of Rm is about 10^{12} , we performed the simulations in the range of Rm higher than $Rm = 10^4$. The highest value of Rm in our simulations was 10^5 .

In this set of simulations we again notice that the amplitudes of the meridional flow are nearly independent of the value of Rm as shown in Fig. 4 (right). The thickness of the tachocline at the equator reduces from $0.030R_\odot$ to $0.015R_\odot$ when Rm is changed from 10^4 to 10^5 , whereas the thickness of the tachocline at the pole goes down from $0.012R_\odot$ to $0.003R_\odot$. Correspondingly, the toroidal field (B_ϕ) in the tachocline region increases from $0.3B_0$ to $1.3B_0$.

4.3. Effect on the Lundquist number

It will be worthwhile to give some emphasis on the choice of the poloidal field strength. In our simulations, we find that the choice of the amplitude of the seed field value is very critical. A small variation in either direction of that value of the magnetic field, which produces a solar-like tachocline, will either make the iso-rotation curves similar to the non-magnetic case or the curves will comply with Ferraro's theorem, unable to produce a tachocline in both cases. At lower values of Pm , we require smaller seed field as shown in Fig. 5. At higher values of Rm , the required value of S_0 is higher (Fig. 6).

An empirical law governing the variation of S_0 as a combined function of Pm and Rm can be deduced from these plots as

$$S_0 \simeq 10 Rm^{0.5} Pm^{0.25}. \quad (10)$$

² The thickness is defined as the distance between the outer boundary and the radius at which the rotation rate deviates by 1% from the rotation rate deep inside the core.

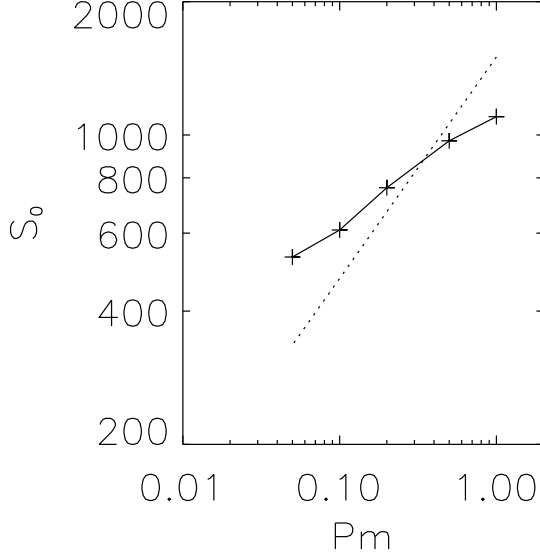


Fig. 5. Variation of S_0 with varying Pm as a log-log plot, for an approximate tachocline thickness of $0.025R_\odot$. The dotted line represents a fixed $Ha = 1500$.

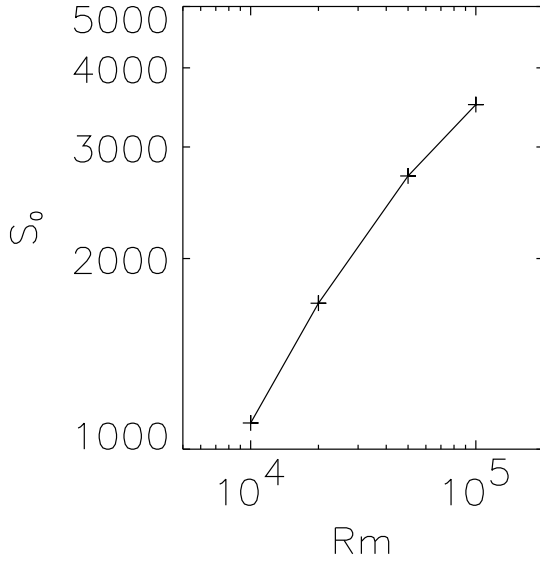


Fig. 6. Variation of S_0 with varying Rm as a log-log plot, for an approximate tachocline thickness of $0.028R_\odot$.

The scaling (10) is the main result of the computations. It means that

$$\frac{B_0}{\sqrt{\mu_0\rho}} \simeq 10^4 \sqrt{\Omega^2 \nu \eta} \quad (11)$$

which, of course, has the correct dimension of a velocity. The old estimation without meridional flow in Kitchatinov

& Rüdiger (1997) led to the quite different expression $B_0/\sqrt{\mu_0\rho} \simeq 10^3 \sqrt{\nu\eta}/R$ which is a very small value due to the appearance of the radius R . Eq. (11) yields

$$\frac{B_0}{\sqrt{\mu_0\rho}} \simeq 10^{-2}, \quad (12)$$

so that a maximum field amplitude of 0.1 Gauss results, for an average density of 10 g/cm^3 . This is a much larger value than the mGauss values for models without meridional flow, but it is not an unrealistic number. Contrary to the old model, now the toroidal field belts have the same order of magnitude than the poloidal fields.

5. Effect of a temperature gradient

In the simulations discussed in the previous sections, we noted that the amplitude of the meridional circulations was nearly independent of the variation of Rm as well as Pm . In the lower latitudinal belt, where the seat of the solar dynamo is located, the amplitude of horizontal velocity (u_θ) was always around 1% of u_ϕ and penetrating deep inside the shell. The Lithium abundance in the Sun, at the base of convection zone, however, suggests that the meridional circulations should either be shallower or slower. To achieve this, we now include a fixed temperature gradient in our model as given. We introduce a temperature fluctuation (Θ) on top of this temperature profile. This fluctuation induces a buoyancy force. Hence Eq. (4) will be modified to

$$\begin{aligned} \frac{\partial \mathbf{u}}{\partial t} = & -(\mathbf{u} \cdot \nabla) \mathbf{u} - \nabla P + \nu \Delta^2 \mathbf{u} + \frac{1}{\mu_0 \rho} (\nabla \times \mathbf{B}) \times \mathbf{B} \\ & + g\rho, \end{aligned} \quad (13)$$

where g is the gravitational acceleration. In the context of the Boussinesq approximation and after rescaling as in Section 2, we obtain a buoyancy force as $\tilde{Ra}\Theta\mathbf{r}$ with the modified Rayleigh number

$$\tilde{Ra} = \frac{g\alpha\beta R_{\text{out}}^3}{\eta^2}, \quad (14)$$

where $\beta = T_{\text{in}} - T_{\text{out}}$ and α is the coefficient of volume expansion. The equilibrium solution obtained from the temperature equation alone is chosen as the mean temperature profile (normalized with its bottom value) and is given by

$$T_0 = \frac{r_{\text{in}}}{r_{\text{out}} - r_{\text{in}}} \left(\frac{r_{\text{out}}}{r} - 1 \right) \quad (15)$$

and the non-dimensional energy equation has the form

$$\frac{\partial \Theta}{\partial t} = \frac{Pm}{Pr} \Delta \Theta - \mathbf{u} \cdot \nabla (\Theta + T_0), \quad (16)$$

where $Pr = \nu/\chi$ is the Prandtl number using the thermal diffusivity χ .

When the model is evolved from the initial state including the temperature equation, it takes much longer (in terms of magnetic diffusion times) to achieve a steady state solution than the simpler cases in the previous sections. To save the computational resources, we fed the

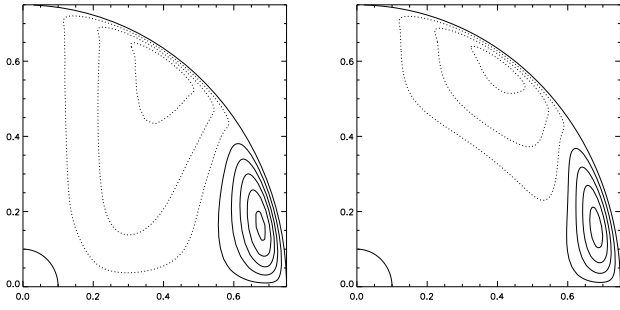


Fig. 7. Results for the simulations excluding (left) and including (right) buoyancy. The solid and the dotted lines are clockwise and anti-clockwise meridional circulations, respectively. $\tilde{Ra} = -2 \times 10^7$, $Rm = 10^4$.

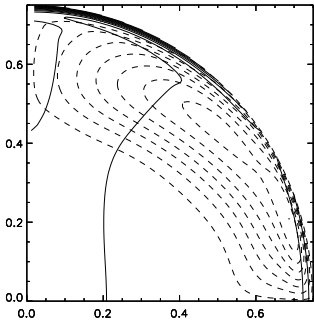


Fig. 8. The same as in Fig. 1 but with buoyancy effect, $Ra = -2 \times 10^7$, $Rm = 10^4$.

steady state solutions obtained in the previous sections as the initial condition for the simulations involving temperatures. It was verified that the solutions obtained in this manner are identical to the solutions obtained in the cases where the temperature equation is included in the evolution from the initial state.

We used $Rm = 10^4$ and $Pm = 1$ for these sets of simulations. As the simulation domain is of radiative nature, we use negative values of \tilde{Ra} . We performed the simulations with various values of \tilde{Ra} . The results are presented in Fig. 7. For the regime when $-\tilde{Ra}/Rm^2 \leq 0.01$, the buoyancy is unable to produce any major change in any of the velocity components in magnitude or in structure. For higher \tilde{Ra} , we see a gradual change in the structure of the meridional circulations³. At higher \tilde{Ra} , the circulations are much shallower for higher latitudes, as desired. The magnitude of the flow also decreases but the change is not drastic (see Fig. 9). For the lower latitudinal belt, which is an important region for the solar dynamo, we see a marginal but definitive decrease in the amplitude of the flows as well as in the depth of the circulations. Similarly, we get a marginal increase in the amplification of the toroidal field. The structure of the toroidal field is changed as well, and it is shifted towards the outer parts of the shell. On the other hand, the rotation rate at higher latitudes, deep inside the

³ Note that $-\tilde{Ra}/Rm^2 \simeq g/(\Omega^2 R)$

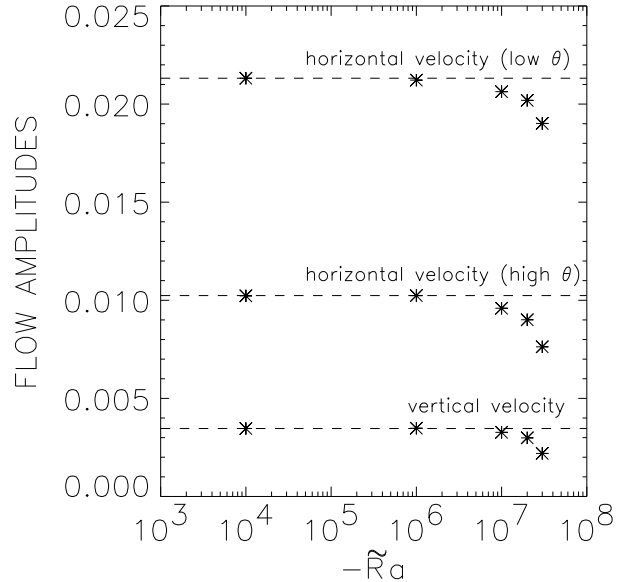


Fig. 9. Plot of the amplitudes of the components of the meridional flow at different co-latitudes (θ), normalized to the rotational velocity at the equator, with varying \tilde{Ra} . The dashed lines represent the corresponding values without buoyancy effect. $Rm = 10^4$, $Pm = 1$.

core, becomes slightly slower than that at the equator. But even this change is marginal and within the observational limits ($|1 - \Omega_{\text{pole}}/\Omega_{\text{equator}}| \leq 3\%$ for $r \leq 0.65R_{\odot}$). This is demonstrated in Fig. 8. We expect that even higher \tilde{Ra} will make the meridional circulations further shallower as well as slower.

6. Summary

In this work, we have presented the first MHD model for the solar tachocline which self-consistently calculates the meridional circulations. The inclusion of the meridional flow changes the shape, the structure and the characteristics of the tachocline radically. Hence, the meridional circulations cannot be neglected while modeling the solar tachocline. The thickness of the tachocline in the outer boundary layer near the equator will be determined by the gradient of the magnetic field near the boundary. Our simulations show that the tachocline is thinner near the pole. But our simulation domain assumes uniform values of viscosity and magnetic diffusivity, it will be only fair to say that we only simulate that part of the tachocline, which is inside the radiative zone. Hence, a definitive conclusion about the thickness of the tachocline in the polar region cannot be drawn from these simulations.

We further report that the tachocline is thinner at lower values of Pm as well as at higher values of Rm . The meridional circulations are nearly independent of the variation in Rm and Pm . The amplification of the toroidal magnetic field is larger at higher values of Rm , whereas

the poloidal magnetic field amplitude required to produce a solar-like tachocline goes down with increasing Rm . The magnetic seed field required to produce a solar-like tachocline is a function of Rm as well as Pm . The value of the seed field is expected to be around 0.1 Gauss in the Sun, for an average density of 10 g/cm^3 . Again a significant change is noted from the simulations without meridional flow where even a sub-mGauss field was enough to produce a solar-like tachocline. The scaling of the magnetic field as a function of the rotation rate ν and η is given in Eq. (11). The toroidal magnetic field is expected to be a few orders higher than the poloidal seed field in case of the Sun.

When a stable temperature gradient is introduced across the shell, it makes the meridional circulations shallower as well as weaker for higher values of the Rayleigh number. This can explain the Lithium abundance as observed in the deeper layers of the solar convection zone, because less Lithium is transported to the Lithium-burning zone below the tachocline. The toroidal magnetic field, in this case, is shifted to the outer parts of the radiative zone.

The relations describing the variation of various parameters such as Lundquist number required to form a solar-like tachocline, the amplification of the toroidal magnetic field, the amplitude of the meridional circulations etc. are based on the simulation results for a limited range of Rm and Pm . We hope to improve the code and verify the correctness of these relations closer to the solar values of Rm and Pm in the near future.

Acknowledgements. L. Kitchatinov is acknowledged for the discussions about the simulation results and H.M. Antia for clarifying the observational results.

References

- Antia, H. M., Basu, S., & Chitre, S. M. 1998, MNRAS, 298, 543, astro-ph/9709083
 Basu, S., & Antia, H.M. 2001, MNRAS, 324, 498, astro-ph/0101314
 Cally, P. S. 2003, MNRAS, 339, 957
 Charbonneau, P., Christensen-Dalsgaard, J., Henning, R. et al. 1999, ApJ, 527, 445
 Charbonneau, P., & MacGregor, K.B. 1993, ApJ, 417, 762
 Dikpati, M., Gilman, P., & Rampel, M. 2003, ApJ, 596, 680
 Eff-Darwich, A., Korzennik, S. G., & Jiménez-Reyes, S. J. 2002, ApJ, 573, 680
 Ferraro, V.C.A. 1937, MNRAS, 97, 458
 Forgács-Dajka, E., & Petrovay, K. 2002, A&A, 389, 629–640, astro-ph/0201241
 Garaud, P. 2001, MNRAS, 324, 68
 Garaud, P. 2002, MNRAS, 329, 1, astro-ph/0108276
 Gilman, P., & Fox, P. 1997, ApJ, 484, 439
 Gough, D.O., & McIntyre, M.E. 1998, Nature, 394, 755
 Hollerbach, R. 1994, Phys. Fluids 6, 2540
 Hollerbach, R. 2000, Int. J. Numer. Meth. Fluids, 32, 773
 Howe, R. 2003, Proc. SOHO 12/ GONG+ 2002, 81
 Kippenhahn, R., & Weigert, A. 1994, Stellar Structure and Evolution. Springer
 MacGregor, K.B., & Charbonneau, P. 1999, ApJ, 519, 911

Miesch, M. 2003, ApJ, 586, 663

Petrovay, K. 2003, Sol. Phys., 215, 17, astro-ph/0303034

Rüdiger, G., & Kitchatinov, L. 1997, Astron. Nachr., 318, 5, 273

Schou, J., Antia, H. M., Basu, S. et al. 1998, ApJ, 505, 390

Spiegel, E.A., & Zahn, J.-P. 1992, A&A, 265, 106

Stix, M., & Skaley, D. 1990, A&A, 232, 234

Watson, M., Astrophys. Fluid Dyn., 161, 285